Review of Scientific Instruments

A 1 kA-class cryogen-free critical current characterization system for superconducting coated conductors

Cite as: Rev. Sci. Instrum. **85**, 113907 (2014); https://doi.org/10.1063/1.4902139
Submitted: 24 September 2014 . Accepted: 03 November 2014 . Published Online: 25 November 2014

N. M. Strickland, C. Hoffmann, and S. C. Wimbush

A 1 kA-class cryogen-free critical current characterization system for superconducting coated conductors

N. M. Strickland,[a] C. Hoffmann,[b] and S. C. Wimbush
The Robinson Research Institute of Victoria University of Wellington, P.O. Box 600, Wellington 6140, New Zealand

(Received 24 September 2014; accepted 3 November 2014; published online 25 November 2014)

A cryogenic electrical transport measurement system is described that is particularly designed to meet the requirements for routine and effective characterization of commercial second generation high-temperature superconducting (HTS) wires in the form of coated conductors based on $YBa_2Cu_3O_7$. Specific design parameters include a base temperature of 20 K, an applied magnetic field capability of 8 T (provided by a HTS split-coil magnet), and a measurement current capacity approaching 1 kA. The system accommodates samples up to 12 mm in width (the widest conductor size presently commercially available) and 40 mm long, although this is not a limiting size. The sample is able to be rotated freely with respect to the magnetic field direction about an axis parallel to the current flow, producing field angle variations in the standard maximum Lorentz force configuration. The system is completely free of liquid cryogens for both sample cooling and magnet cool-down and operation. Software enables the system to conduct a full characterization of the temperature, magnetic field, and field angle dependence of the critical current of a sample without any user interaction. The system has successfully been used to measure a wide range of experimental and commercially-available superconducting wire samples sourced from different manufacturers across the full range of operating conditions. The system encapsulates significant advances in HTS magnet design and efficient cryogen-free cooling technologies together with the capability for routine and automated high-current electrical transport measurements at cryogenic temperatures. It will be of interest to both research scientists investigating superconductor behavior and commercial wire manufacturers seeking to accurately characterize the performance of their product under all desired operating conditions. © *2014 AIP Publishing LLC*. [http://dx.doi.org/10.1063/1.4902139]

I. BACKGROUND

State-of-the-art second generation coated conductors based on the high-temperature superconductor (HTS) $YBa_2Cu_3O_7$ (YBCO) are presently available on a commercial basis from a number of manufacturers, for example, American Superconductor,[1] SuperPower,[2] Fujikura,[3] Superconductor Technologies,[4] and Bruker HTS,[5] with a substantial number of additional companies aspiring to offer similar products in the near future. Such superconducting wires are anticipated to have wide-ranging applications in the fields of sustainable energy (wind turbines, efficient motors, and generators),[6] power infrastructure (transformers, fault current limiters),[7] medical devices (magnetic resonance imaging),[8] and large scale scientific facilities (ITER fusion reactor, particle accelerators),[9] as well as for the creation of inserts for high field strength electromagnets.[10] However, the vision of operation at liquid nitrogen temperatures (65–77 K) is no longer considered feasible for many of these applications where the superconductor must be situated in a magnetic field, due to performance limitations of the material. Instead, operation at lower temperatures (e.g., 30 K for 3 T) is now being mooted.

Most characterization of superconducting wire performance is conducted at 77 K due to ease of operation and the elimination of the requirement for liquid helium based cooling systems. However, recently it has been becoming more and more apparent that 77 K characterizations tend to be meaningless when extrapolated to significantly lower temperatures. Indeed, it has most recently been shown that a wire that operates better at 77 K than another may in fact perform *worse* in absolute terms when the comparison is repeated at 20 K.[11] There is consequently both a desire and a need to perform superconducting wire characterization at the actual operating temperatures of relevance to the final application, both from the point of view of obtaining accurate performance data to inform device design and from the scientific viewpoint of understanding the true performance of technological superconducting materials. At the same time, a return to liquid helium based measurement systems is impractical and inconvenient for research scientists, and practically impossible for industrial technicians. Furthermore, state-of-the-art superconducting wires have low-temperature performance that is beyond the capability of the majority of available laboratory-based systems to adequately characterize. There is thus a strong demand for a new class of instrument that directly addresses these issues.[12,13]

II. SYSTEM OVERVIEW

The system is built around an 8 T HTS magnet available commercially from HTS-110 Ltd.[14] The magnet is a compact

[a]Author to whom correspondence should be addressed. Electronic mail: nick.strickland@vuw.ac.nz.
[b]Present address: Ceraco Ceramic Coating GmbH, Rote-Kreuz-Str. 8, D-85737 Ismaning, Germany.

split-coil transverse field design wound around an iron core to provide field enhancement and improved field homogeneity across the sample volume at the expense of a nonlinear dependence of the magnetic field strength on coil current. The room-temperature bore has a diameter of 30 mm with an extended central slot, allowing for an insulated variable temperature insert of diameter 22 mm as well as external gas lines. The bore is vacuum tight and therefore acts directly as the outer wall of the insert cryostat. The magnet is conduction cooled to 15 K using a Sumitomo CH-208L cryocooler powered by a HC-8E4 compressor. Power to the magnet coil is provided by a pair of programmable bipolar dc power supplies (Kepco BOP 6-125MG) connected in parallel to provide up to 250 A, with ±210 A being the coil current required for ±8 T operation. A calibrated Hall sensor (Arepoc LHP-NP) situated between the poles immediately outside the sample space allows measurement and control of the applied magnetic field via a Lake Shore Model 475 DSP Gaussmeter.

A schematic showing the various components of the system and how they interrelate is shown in Figure 1, alongside a photograph of the complete system. A vacuum chamber, mounted above the bore of the magnet, contains the sample cooling sub-system comprising the variable temperature insert, a second cryocooler, and the cold parts of the circulating-gas sample-cooling system. The sample cryocooler is a Sumitomo CH-204S powered by a HC-4E1 compressor. This was chosen for compactness and commonality with the magnet cooling system, and in particular with a view to running both cold heads from a single compressor, although that was not attempted here. Both cryocoolers were operated at 50 Hz electrical mains frequency and would deliver a greater cooling capacity if operated at their design frequency of 60 Hz. The CH-204S cryocooler is a relatively low-specification model and the system could readily be modified to incorporate a more powerful model in order to reach a lower base temperature. The system thus offers significant scope for expansion and development towards other materials systems of interest, in particular MgB_2.

The cold head temperatures, sample space temperature, and actual sample temperature are all monitored and controlled by a Lake Shore Model 336 Cryogenic Temperature Controller. This controller provides for dual control over two 22 W resistive heaters mounted on the sample rod and at the inlet of the variable temperature insert giving precision sample temperature control to better than ±0.01 K. A Lake Shore Model 218 Cryogenic Temperature Monitor provides a readout of up to eight diagnostic temperature sensors embedded within the cooling system.

The sample insert is capped with a slip-sealed rotation stage (PI miCos DT-80 with 041 stepper motor and SMC Pollux motor controller) that allows for direct rotation of the sample rod within the transverse field of the magnet, maintaining the constant (maximum) Lorentz force configuration of current flow perpendicular to magnetic field.

Electrical current for the current-voltage (*IV*) characteristic measurement that constitutes the heart of the system is supplied by an Agilent 6680A dc power supply. The model used provides up to 875 A, although a special order version is available to deliver 1 kA. The actual instantaneous current supplied to the sample is measured across a precision 0.1 mΩ power resistor included in the current circuit. The voltage signal from the sample passes through a custom-built nanovolt amplifier with a gain of 10 000 before being read using a National Instruments USB-6211 multifunction data acquisition module.

The system is operated using a custom LabVIEW™-based software package running on a standard desktop PC. Communication between instruments and the PC is via GPIB (National Instruments GPIB-USB-HS) and RS-232 interfaces. The system is fully automated and under normal conditions the software controls all aspects of system and magnet operation, as well as acquiring measurement data and fitting

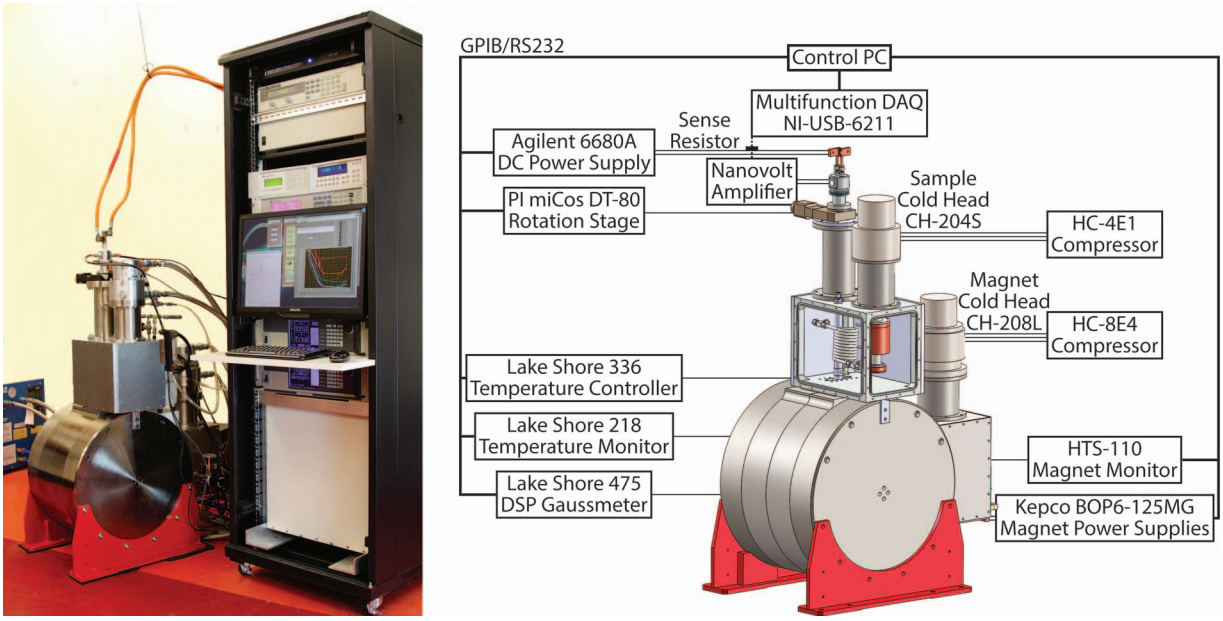

FIG. 1. Photograph and schematic of a cryogen-free critical current characterization system for coated conductors.

the data to obtain the critical current, I_c, and power-law index, n. User intervention is required only to exchange samples and to set up and initiate a measurement program.

III. DESCRIPTION OF MAJOR COMPONENTS

There are a number of novel components of the system that are key to its successful operation, and these are described in detail below.

A. Circulating gas sample cooling system

Figure 2 shows a detailed schematic of the sample cooling system.[15] Under normal operation, the gas inlet valve and vacuum valve are closed giving a closed-cycle system circulating technical grade helium gas at an overpressure of typically 0.3 bar. The 0.1–0.2 bar circulation pressure differential for the helium gas is provided by a (sealed) diaphragm pump (KNF Neuberger N022 AN.18) operating at or above ambient temperature. The room-temperature gas is pre-cooled by passing through the cooling side of a cryogenic recuperator (Sec. III B) and is then cooled successively by a pair of copper heat exchangers mounted on the first and second stages of the cryocooler (Sec. III C). From there it passes into the base of the variable-temperature insert situated within the bore of the magnet and directly cools the sample and the lower section of the current leads. The gas is withdrawn part-way up the insert, passes through the heating side of the cryogenic recuperator, and is returned to the pump. The flow valve allows for control of the flow rate of the gas, which is measured by a rotameter (Omega Engineering FLDA3421ST) and typically held at 6–9 standard liters per minute.

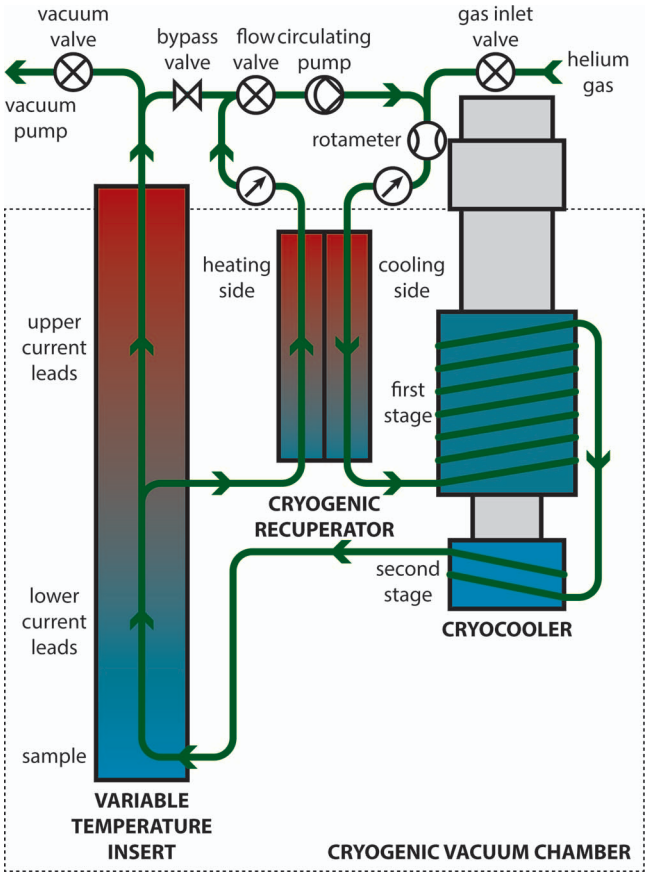

FIG. 2. Detailed schematic of the cryogenic circulating helium gas sample cooling system.

Operating the gas cycle in this manner allows for the lowest base temperature at the bottom of the variable-temperature insert to be achieved. However, with a sample rod in place, the substantial heat leak down the high-current leads from room temperature limits the base temperature of the *sample*. Achieving the lowest possible sample temperature would involve designing the position of the gas return line on the insert to provide optimized cooling of the current leads. However, this optimized position will depend on the nature of the sample rod/current leads and on the gas flow rate and the gas line position is clearly not conveniently adjustable. An alternative method of optimizing the cooling is to introduce an alternative gas pathway bypassing the recuperator. Here, a fraction of the cooling gas (controlled via a needle valve) passes up the full length of the sample insert, cooling the current leads along their entire length such that the sample reaches a minimal base temperature. As an approximate guide, the fraction of gas flowing through the bypass is set such that the gas exiting the sample insert via this route has just reached room temperature, i.e., the full available cooling power of the gas has been applied to the sample leads. The gas then rejoins the closed circuit at the pump.

Sample exchange is accomplished, while the variable temperature insert remains cold by opening the gas inlet valve connected to a helium gas cylinder. This provides a flow of helium gas through the cold heat exchangers to the variable-temperature insert ensuring minimal backflow of contaminant gases into the system. In conjunction with the gas inlet valve, the vacuum valve connected to a small rotary vacuum pump (Edwards E2M1.5) allows for evacuation and backfilling of the system to remove residual contaminant gases.

Initial cool-down of the variable temperature insert from room temperature takes around 2 h (Figure 3(a)). Once the insert is cold, cooling of a sample to low temperature following exchange takes as little as 30 min (Figure 3(b)), or less if an intermediate temperature (e.g., 77 K) is sufficient to begin measurement. The entire system including current leads continues cooling to equilibrium over a period of 1–2 h, after which the minimum sample temperature is achieved.

B. Cryogenic recuperator

To solve the challenge of circulating a gas at cryogenic temperatures, a number of options are available. Conceptually, the most simple is the use of a cryogenic fan to pump the gas in an entirely low-temperature closed loop. Such devices are commercially available;[16] however, they are costly and hard to maintain. The alternative, employed here, is to bring the gas to room temperature in order to pass it through a standard gas displacement pump, returning it to the cryogenic environment after it leaves the pump. Implemented directly, this would be extremely wasteful of the cooling capacity of the gas, with much of its cooling power being lost to the

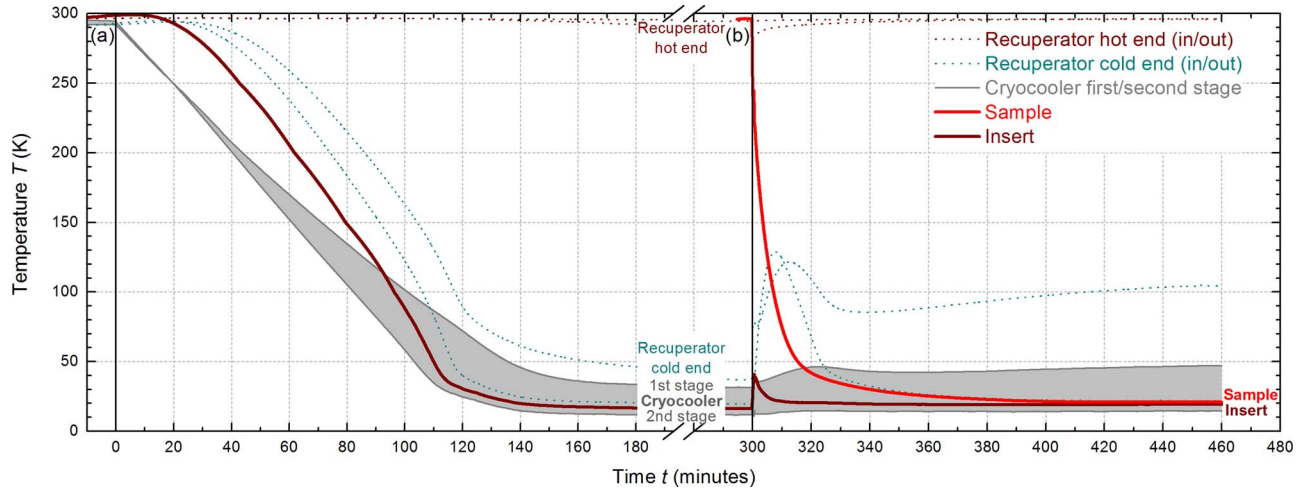

FIG. 3. Plot showing cool-down curves of sample cooling system components from room temperature: (a) empty insert, (b) following sample rod insertion.

ambient environment. It is therefore beneficial to incorporate a cryogenic recuperator[17] into the cooling cycle in order to gainfully extract the residual cooling power of the gas being taken to room temperature by using it to cool the returning gas flow. This simple idea has the potential, in principle, to avoid any loss of cooling power whatsoever in this process. Measurements on our system show that our design comes close to this ideal.

Our cryogenic recuperator design (Figure 4) is a tube-in-tube counter-flow arrangement having a 3/16 in. copper tube running within a 5/16 in. stainless steel tube. This approximates to equal gas volumes in the internal and external pathways. The use of a copper internal tube ensures good heat transfer between the hot and cold gases, while the use of a stainless steel outer tube, with much lower thermal conductivity, limits the heat conduction along the length of the recuperator linking the hot and cold ends. The concentric pair of tubes is bent into a helix, the overall tube length being around 2.5 m. The two ends are terminated by brazing or welding into modified Swagelok® 1/4 in. T-pieces appropriately drilled out such that the flow through the inner tube passes out through the straight edge, while the annular flow through the outer tube emerges from the perpendicular coupling.

In tests performed with the bypass line closed and the gas flow set at the standard rate, at equilibrium the cold end of the recuperator maintains a temperature difference of 18 K (as shown in Figure 3). Relative to the highest temperature of the gas cycle being room temperature for operation of the pump, this represents an efficiency of 93% in recovery of the cooling power of the cold gas. However, the temperature difference at the warm end of the recuperator under this condition is 12 K. Thus of the 7% loss in cooling power, only one third represents actual losses (heat gained from the environment) in the recuperator, while two thirds represents incomplete heat exchange. The latter could be improved by increasing the length of the recuperator, although losses are expected to be inversely proportional to the length of the tube so gains would be small for incremental increases in length.

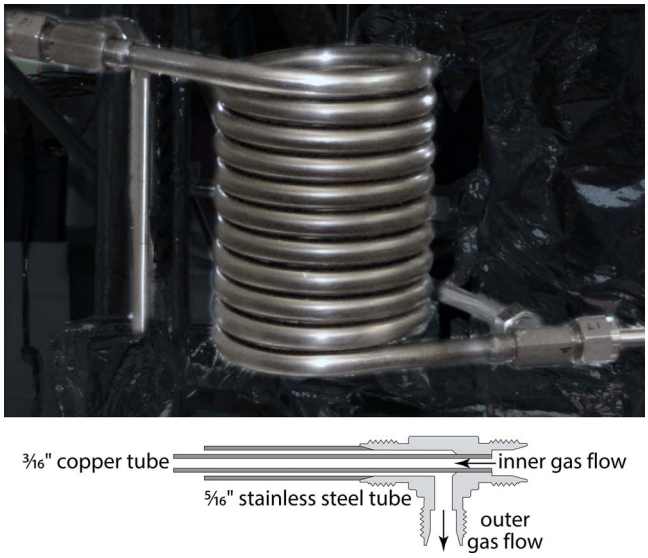

FIG. 4. Photograph of the cryogenic recuperator and schematic of the terminating Swagelok® connection.

C. Cryocooler heat exchangers

Transfer of heat between the helium gas and the cryocooler is achieved using copper heat exchangers, as shown in Figure 5. Efficient heat exchange requires that the path length for the gas in the heat exchanger be sufficiently long for the gas temperature to equilibrate to the temperature of the copper body. For the heat exchanger on the first stage of the cryocooler we employed a helical path machined into one of a pair of concentric sleeves, while for the second stage we employed a multiple-layer serpentine path. The separate parts were soldered together to achieve a vacuum-tight gas seal. These two approaches enable us to achieve a gas-flow path length of around 2 m within a compact body in each case. In each case the outgoing gas is at the top, closest to the cryocooler, to achieve the lowest possible gas temperature. A small spiral heat exchanger was also employed at the inlet to the variable temperature insert allowing the incoming gas to be heated to provide a coarse temperature control. Due to their low operating temperatures, for best performance each

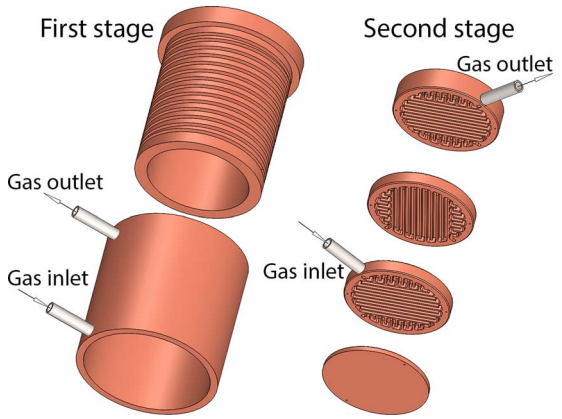

FIG. 5. Design of first and second stage cryocooler heat exchangers for efficient gas cooling.

of these heat exchangers should be made from high thermal conductivity (OFHC) copper.

D. High-current sample rod

The rod that supports the sample within the variable temperature insert must possess three important characteristics. Fundamentally, the current leads must be able to carry the current to be delivered to the sample, in this case up to a kiloamp, with minimal heat generation. This calls for thick rods of a high electrical conductivity material. On the other hand, these current leads must also transport as little heat as possible from their room temperature end to the sample, calling for thin rods of a low thermal conductivity material. For metals the thermal and electrical conductivities are directly related through the Wiedemann-Franz law so these two requirements are in direct conflict and must be balanced carefully. One way to circumvent the Wiedemann-Franz law is to use HTS wires on the cold end of the current leads. These can carry some or all of the required current with negligible heat generation, while having a relatively low thermal conductance.[18] The third requirement is for sufficient mechanical strength to support rotation of the superconducting sample (and superconducting current leads) within a strong magnetic field, against flux trapping and Lorentz force effects. The simultaneous satisfaction of these requirements, along with the size constraints of the variable-temperature insert, means that the sample rod is one of the most complex mechanical parts of the system.

We provide electrical conductivity for the low duty-cycle current ramp through the use of a 0.12 mm thick copper foil, rising to 0.42 mm at the hot end of the sample rod (where the electrical resistance of the copper is higher). To reduce instantaneous heating in the vicinity of the sample, we supplement this with two 4 mm wide HTS wires soldered to the copper surface of each lead at the low temperature end. We have used both first generation (Sumitomo) and second generation (AMSC and Fujikura) wires with good effect. By providing this zero-dissipation pathway for the electrical current near the sample, we ensure that most of the Joule heating is localized some distance away, enabling the measurement to complete with only small temperature excursions (see below).

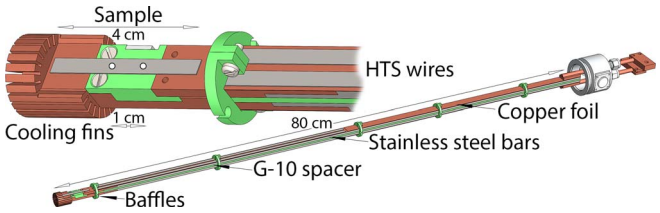

FIG. 6. Technical drawing of the high-current sample rod, indicating the materials used in its construction. The inset shows a detailed view of the sample holder end.

A side effect to be considered though is that flux-trapping forces act on the parts of these HTS tapes that are within the magnetic field, resisting rotation. The flux-trapping force is proportional to the critical current of the tapes and it is therefore important that these be chosen to have an appropriate current rating. Structural and torsional stability is provided by a 3 mm thick non-magnetic stainless steel bar to which the copper foils are soldered. Compared to copper, stainless steel offers far greater strength with much reduced thermal conductivity. The 12 mm wide positive and negative current leads are bolted together sandwiching a G-10 glass-reinforced epoxy laminate insulating spacer to further increase the strength of the assembly. The sample mount is a solid block of oxygen-free high conductivity copper with fins to provide improved cooling. The entire sample rod assembly is depicted in Figure 6.

The sample is soldered in place across the two current leads using a low-temperature In-Bi solder to avoid damage to the superconductor due to excessive heat application. Good electrical contact is required to prevent Joule heating at the contacts and to ensure effective current transfer into the superconductor sample. Voltage leads are soldered to the sample surface, and a calibrated Cernox™ temperature sensor glued to a sapphire plate is wire clamped on to the sample using a thin coating of Apiezon® N grease to ensure an accurate temperature measurement while also securing the sample against movement. The sample mount, and the sample rod itself, must be able to withstand a significant Lorentz force acting to twist it within the magnetic field when high currents are passed through it. As these forces can exceed 300 N at a field of 8 T while passing 1 kA through a sample of 4 cm length, unlaminated samples must be securely clamped in place against the sample rod to prevent this. In addition to the Lorentz force, flux trapping produces a significant restraining force within a magnetic field, independent of any current flow. This leads to a restraining torque on the sample as the sample rod is rotated to change the field angle, with unreinforced samples easily bending to destruction if not securely clamped in place. The sample rod is supported at its upper end a distance of 80 cm away and, despite its rigid construction, readily deflects to an angle of several degrees under this torque. This leads to an error in the field-angle setting necessitating an independent measurement of sample orientation as described in Sec. III E.

The sample rod design presented here passes 875 A at 30 K with a temperature rise of less than 0.25 K on the sample throughout the duration of the measurement up to the critical current. This temperature rise scales as the square of the

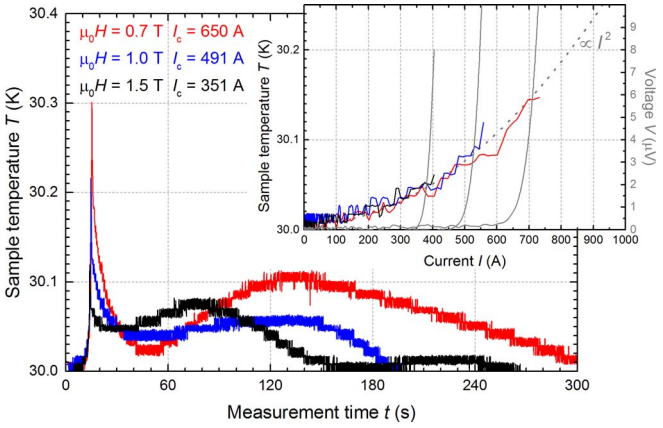

FIG. 7. Sample temperature changes upon conducting *IV* curve measurements at 30 K under varying applied fields in order to achieve critical current values ranging from 350 A to 650 A. The inset shows the sample temperature rise overlaid with the voltage signal throughout the duration of the current ramp, while the main panel shows the long-time evolution of the sample temperature. The initial, sharp rise in temperature during the measurement is due to Joule heating at the sample contacts, while the delayed temperature peak is caused by heat conduction down the current leads.

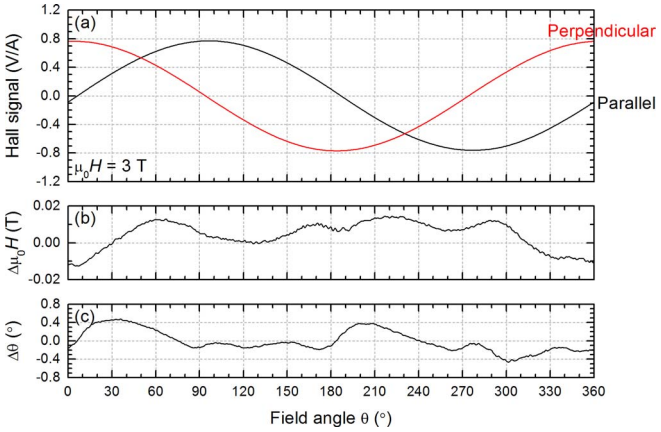

FIG. 8. (a) Raw signal output of orthogonally mounted Hall sensors in dependence on the applied field angle at 3 T, and derived (b) magnetic field and (c) field angle readout deviations from their respective setpoints.

current, as seen in the inset of Figure 7, and for example is less than 0.05 K at 400 A. The main plot of Figure 7 shows a sharp initial temperature rise in the first 15 s associated with heat generated near the sample (most likely in the transfer of current through the contacts into the sample). The temperature continues to rise for ∼0.2 s after completion of the current ramp as heat continues to flow in from the ends of the sample. In the 0.7 T curve, for example, the temperature rise presented in the inset is 0.15 K at the end of the current ramp (and slightly less at I_c), but we can see from the main plot that the temperature rise continues to 0.30 K after the measurement. With the temperature sensor well thermally anchored to the sample, the true delay associated with heat transfer along the sample is expected to be much greater than artefact delays associated with heat transfer to the sensor. On a longer time scale of a minute or more, a second temperature peak results from heat conducted from the warmer parts of the current leads that are subjected to stronger Joule heating. This temperature rise is partially damped by the action of the temperature controller.

Compared to the base temperature of 16 K of the empty insert, the heat leak created by the inclusion of the sample rod, cooled using the optimally-set recuperator bypass, increases the temperature of the insert to 19 K (Figure 3). This is sufficient to stabilize the temperature of the sample at 21 K. Convenient automated measurements can be conducted at 25 K, where the available temperature buffer counters accumulated Joule heating of the warmer part of the current leads.

E. Field angle measurement

Two embedded Hall sensors (Arepoc LHP-NP) mounted orthogonally within the G-10 spacer directly behind and to the side of the sample provide a continuous readout of both the magnitude and the direction of the applied field at the sample (Figure 8). Field inhomogeneity between the two sensors limits the accuracy of the field readout at an arbitrary angle to typically ±0.5%. The accuracy of the angle readout is not greatly affected by minor deviations in the field magnitude between the sensors, and consequently is better than ±0.5° over the full angular range. This reading can be used to correct for angular deviations due to the torque exerted on the sample rod by the sample in a magnetic field as described in Sec. III D.

F. Safety features

The current leads both comprising the sample rod and connecting to it are not rated for continuous operation at 1 kA dc, and indeed this would be undesirable for a number of practical reasons: an excessive heat leak into the sample space, and a cumbersome rotation and suspension mechanism of the external current leads. A typical measurement involves ramping the current over a period of less than a minute, and tests have shown that such ramps can proceed safely continuously and indefinitely. However, the use of underrated cables carries a risk should a fault condition occur. This risk is effectively mitigated through the incorporation, both on the sample rod and within the external current circuit, of a passive thermostatic switch that triggers a hardware interlock on the power supply, cutting power immediately if the temperature of the leads rises above 50 °C, well within their rated operating temperature.

The circulating gas system is equipped with a 0.8 mbar overpressure release valve for the controlled release of any gas overpressure that arises due to a change in temperature, fault in regulation or user error.

IV. MODEL OF GAS-FLOW COOLING

We can analyze an idealized helium gas-flow cooling circuit to determine the optimum gas flow rate for providing cooling to the sample and current leads in such a way as to minimize the sample temperature.

The gas-flow cooling circuit is shown schematically in Figure 9(a). Gas enters the cryocooler with temperature T_R, is cooled sequentially by the first and second stages of the

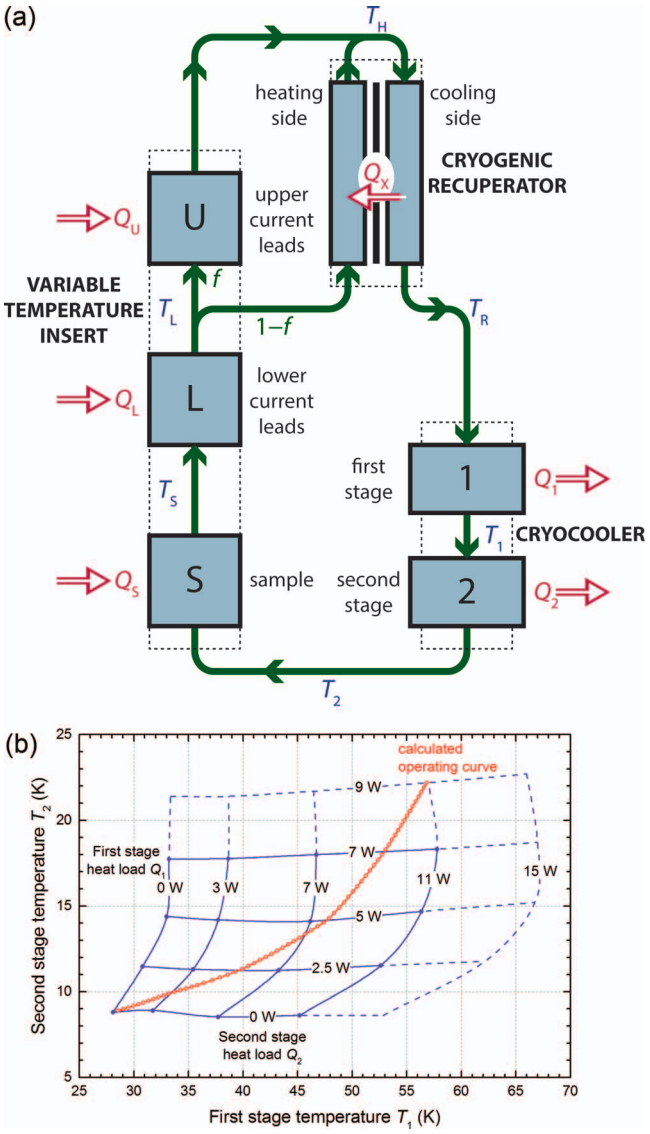

FIG. 9. (a) Gas-flow cooling circuit, showing each stage of heat transfer and the gas temperatures between stages. (b) Cooling capacity map for the CH-204S cold head operating at 50 Hz, showing how T_1, T_2, Q_1, and Q_2 are interrelated. The manufacturer's 50 Hz specifications[19] (solid lines) have been extrapolated (dashed lines) using the more extensive 60 Hz specifications as a guide. The operating condition of the cryocooler under the range of helium gas flow conditions calculated for Figure 10 is depicted in the curve of open points.

cryocooler, then passes to the variable temperature insert to cool the sample and the lower part of the current leads. At a point partway up the current leads there is a division in the flow. The majority of the gas is warmed by passing through the heating side of the recuperator, while a fraction f of the gas is used to cool the upper part of the current leads. The two gas streams recombine at the circulation pump at room temperature and then pass through the cooling side of the recuperator, precooling back to the temperature T_R to return to the cryocooler. In modeling the heat transfer, we assume that all the heat exchangers are ideal, that is that the gas temperature equilibrates with the heat exchanger temperature by the time it leaves the heat exchanger, and that there is no heat exchange with the environment. For each heat exchange element we can write the equation

$$\dot{Q} = \dot{m} C_p (T_{out} - T_{in}), \tag{1}$$

where $\dot{Q}$ is the rate of heat transfer to the gas (in W), $\dot{m}$ is the mass flow rate of the helium gas through the heat exchanger (in g/s), C_p is the specific heat capacity of helium gas (in J/g K), and T_{in} and T_{out} are the temperatures of the gas entering and leaving the heat exchanger (in K). The specific heat capacity of helium gas is very nearly constant at $C_p = 5.2$ J/g K over the temperature and pressure ranges of interest and for a closed-cycle system the mass flow rate must be the same through each element except where the gas stream divides in which case the reduced flow rates $f.\dot{m}$ and $(1\text{-}f).\dot{m}$ are used. Thus we can write

$$\dot{m} C_p = \frac{Q_1}{T_1 - T_R} \tag{2a}$$

$$= \frac{Q_2}{T_2 - T_1} \tag{2b}$$

$$= \frac{Q_S}{T_S - T_2} \tag{2c}$$

$$= \frac{Q_L}{T_L - T_S} \tag{2d}$$

$$= \frac{Q_U}{f(T_H - T_L)} \tag{2e}$$

$$= \frac{Q_X}{(1-f)(T_H - T_L)} \tag{2f}$$

$$= \frac{Q_X}{T_H - T_R}. \tag{2g}$$

The temperatures and heat transfers at the first and second stages of the cryocooler are further constrained to be compatible with the cooling capacity map shown in Figure 9(b). This map relates the quantities T_1, T_2, Q_1, and Q_2 such that knowing any two in principle fixes the other two. In practice from the map given we can most conveniently extract the dependences $T_1(Q_1,Q_2)$ and $T_2(Q_1,Q_2)$.

To proceed with the analysis we fix the quantities T_H (room temperature) and T_S (the target sample temperature). T_L (the temperature at which the gas stream is divided) and f (the fraction of flow diverted to the upper current leads) are treated first as fixed parameters. From Eqs. (2f) and (2g), we obtain T_R, the gas temperature input to the first stage of the cryocooler, after precooling by the recuperator

$$T_R = f T_H + (1-f) T_L. \tag{3}$$

The quantities f and T_L can therefore be balanced off against each other to determine T_R. Physically, once we know T_R and the mass flow rate $\dot{m}$ this is sufficient to determine the cryocooler operating conditions and thence the cooling power available at the sample and the lower current leads.

In practice, we cannot readily fix or adjust T_L; the point at which the gas flow divides is fixed in physical space along the variable temperature insert and the temperature at this point will depend on the flow rate and current lead heat leaks. However, we can readily adjust the bypass gas fraction f as a proxy for T_L.

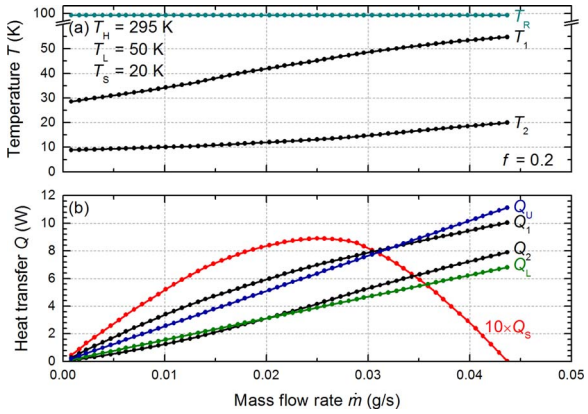

FIG. 10. (a) Modeling of cryocooler first and second stage operating temperatures as a function of helium gas mass flow rate under the stated operating conditions. (b) Cooling power available at various heat transfer points as a function of helium mass flow rate.

The main parameter to be optimized is the helium gas mass flow rate $\dot{m}$. Choosing $\dot{m}$ we can balance Eqs. (2a) and (2b) with the dependences from the cooling capacity map to determine the self-consistent cryocooler parameters T_1, T_2, Q_1, and Q_2. The remaining heat transfer quantities Q_S, Q_L, Q_U, and Q_X can be calculated from Eqs. (2c)–(2g).

The results of the analysis are illustrated in Figure 10. Here the target sample temperature has been chosen as T_S = 20 K, room temperature set to T_H = 295 K, the temperature of the gas at the flow dividing point T_L = 50 K and the flow fraction passing by the upper current leads f = 0.2. With increasing flow rate $\dot{m}$ there is increasing load on the cryocooler resulting in higher operating temperatures (Figure 10(a)), however the higher gas temperature is countered by the greater mass flow, giving a peak in the cooling power available to the sample at 20 K of 1.1 W at a mass flow rate of 0.03 g/s (7.8 L/min) (Figure 10(b)). At that flow rate there is also 7.8 W and 4.7 W of cooling power available to the upper and lower parts of the current leads, respectively. The flow rate of 7.8 L/min is readily achievable with a compact diaphragm pump such as the KNF Neuberger N022 AN.18 used here, confirming that gas-flow cooling is in principle a practical method for transferring heat to the cryocooler at a rate that is well matched to typical cryocooler capacity. In practice, a flow rate on the higher side of the Q_S curve might better optimize the sample temperature as there is a large gain in cooling of the current leads for a small reduction in cooling of the sample. The details of calculating this optimization are complex and depend strongly on the nature of the current lead construction and geometry.

V. EXPERIMENTAL PRINCIPLES

The measurement consists of stepwise ramping of the current through the sample while monitoring the voltage drop across it, until a particular voltage criterion (typically specified as an electric field of 1 μV/cm) is reached, which serves to define the critical current. The resulting $V(I)$ dependence is usually modeled as a power law of the form

$$V = V_c \left(\frac{I}{I_c}\right)^n, \tag{4}$$

where V_c is the specified voltage criterion, and the critical current I_c and exponent n are determined from a power law fit to the data performed in the region close to I_c.

For many measurements of commercial wire samples, the critical current can be hundreds of amps and therefore one of the most important aspects of the experiment is to minimize the Joule heating in the current leads and at the sample, particularly in its contacts. This can best be achieved, regardless of setup, by making the current ramp as brief as possible. On the other hand, a sufficient number of data points must be collected, particularly in the region of I_c, to allow accurate determination of I_c and n. The selection of a preferred ramp rate accommodating these two conflicting requirements is further complicated by the fact that the I_c values to be measured vary over several orders of magnitude even for a single sample due to the strong, and often unpredictable, dependence of I_c on temperature T and applied magnetic field H. The strategy adopted in this experiment is not to attempt to predict the required current, and therefore to use the same current ramp for every measurement. This can be accomplished while still minimizing the heat generation and measurement time by the use of nonlinear current ramp steps using a power law dependence

$$I_n = r^n - 1, \tag{5}$$

where r is a user-definable ramp rate parameter typically in the range 1.010–1.100. Under this approach, at currents much above 1 A the current increments by the same relative fraction (1%–10%) at each step so that the relative density of data points at the high-current end of the ramp $\Delta I/I$ remains approximately constant for all values of I, eliminating the need to estimate I_c beforehand. The voltage across the sample V is recorded and analyzed in real time so that the ramp can be stopped when an appropriate voltage, typically several times V_c, is reached.

The aim of the experiment is to determine $I_c(T,H,\theta)$ and $n(T,H,\theta)$ over an appropriate region of the parameter space. This process is automated by preparing a batch file specifying the range of parameter values desired for each set of measurements, which are then stepped through by the measurement software automatically. Under typical conditions, the system is capable of performing around 4000 IV curve measurements in a 24-h period, while the sample can remain cold indefinitely.

VI. EXEMPLARY RESULTS

Using the system, we have characterized a wide range of superconducting wires obtained from multiple manufacturers as well as research samples produced in-house and obtained from collaboration partners. By way of exemplifying the caliber of results that can be obtained, we present below typical data across the range of capability acquired on one such wire. The full data set is publically available.[20] The sample is a 4.4 mm wide brass-laminated Ag-stabilized YBCO coated

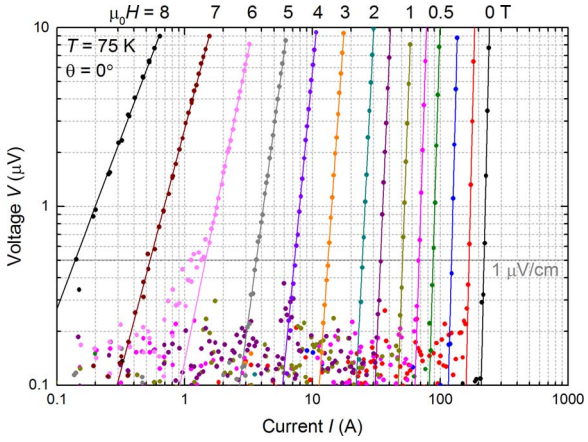

FIG. 11. *IV* curves measured at 75 K under a varying out-of-plane magnetic field on a HTS coated conductor wire. Solid lines are fits to Eq. (4) with the voltage criterion for determination of I_c indicated by the broken line.

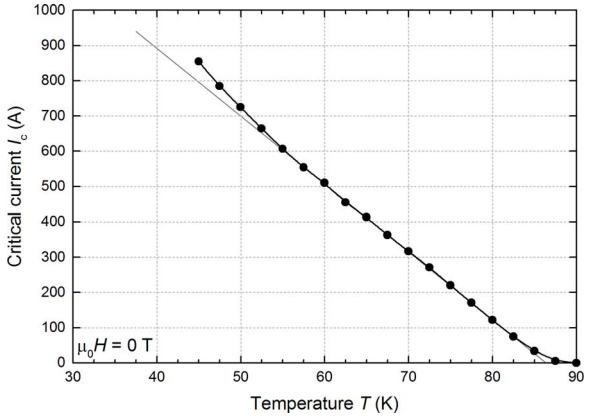

FIG. 12. Self-field temperature dependence of the critical current of an HTS coated conductor wire.

conductor tape cut to 4 cm in length. The sample was soldered in place on the sample rod and voltage taps attached a distance of 5 mm apart in the center section of the sample. A standard suite of characterization measurements was performed on the sample in a batch measurement lasting approximately 48 h.

A. *IV* curves

A typical set of *IV* curves obtained for the sample in a varying out-of-plane magnetic field is shown in Figure 11. The noise floor in the voltage measurement is around 0.2 μV, better than required to ensure a reliable estimate of I_c using an electric field criterion of 1 μV/cm over a voltage tap distance of 0.5 cm. I_c values ranging over four orders of magnitude are determined from fits to the data in accordance with Eq. (4), while the n-value is seen to increase steadily with I_c from a value as low as 2 at 8 T to a value as high as 31 at 0 T for this single data set.

B. Temperature dependence of I_c

The self-field temperature dependence of the critical current of the sample is plotted in Figure 12. From the measured I_c value of 171 A at 77.5 K, it is seen that our measurement of the sample confirms a short-length performance consistent with typical specifications. At temperatures below 45 K, the self-field I_c of the sample exceeds our capability to measure. Also evident in the data is an upturn in performance at temperatures below 55 K of relevance for low temperature applications.

C. Field dependence of I_c

Superconductors typically show a suppression of critical current with applied field strength. Figure 13, plotted logarithmically, shows a plateau region at low fields, followed by a power law decay across much of the field range before I_c drops off sharply on approaching the irreversibility field. Such a behavior is highly typical. Furthermore, a strong anisotropy is observed in the I_c values obtained for fields applied within the plane of the sample ($\theta = 90°$) and out of the plane ($\theta = 0°$), that is again typical of this material.

D. Field angle dependence of I_c

The most detailed measurements acquired using the system are full angular dependences of I_c for fields applied at all azimuthal angles with respect to the transport current in the superconductor. Such measurements are of particular importance for application since a given design is ultimately limited by the lowest value of I_c that the superconductor can support, and often, as is the case here, this may not be in either of the two principal field directions shown in Figure 13. The data of Figure 14 reveals that the angle of minimum I_c for a single sample can range anywhere from a few degrees to the side of the large *ab* ($\theta = 90°$) peak all the way to the *c*-axis ($\theta = 0°$) direction, while the minimum I_c value itself is as much as 30% lower than its value in either of the principal crystallographic directions.

The angle dependence of I_c is specifically related to the geometry of the microstructural defects that provide flux pinning and can vary greatly in form between samples of

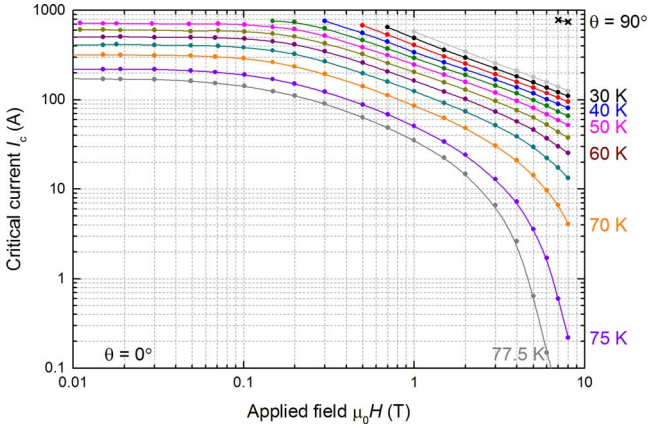

FIG. 13. Field dependence of the critical current of a HTS coated conductor wire measured over a range of temperatures, highlighting the strong anisotropy between fields applied within ($\theta = 90°$) and out of ($\theta = 0°$) the plane of the sample at 30 K. The 75 K I_c values are extracted from the *IV* curves shown in Figure 11.

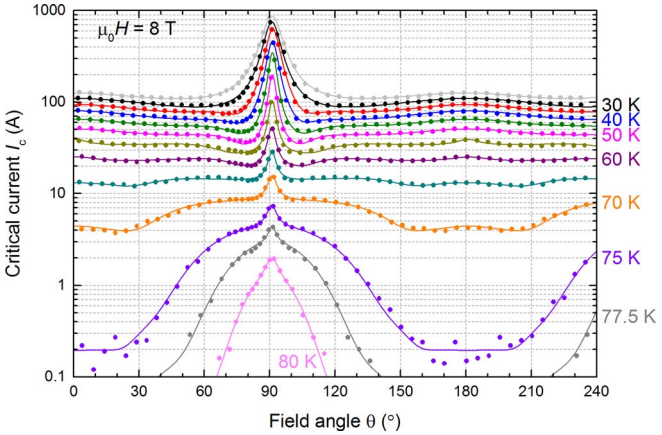

FIG. 14. 8 T field angle dependence of the critical current across a range of temperatures of a HTS coated conductor wire. Solid lines are four-component maximum entropy models of the data.[22]

nominally the same material. Detailed measurements such as those shown on Figure 14 can be related directly to the various microstructural features revealed by transmission electron microscopy and provide guidance in engineering performance-enhanced materials.[21]

E. *n* value

A somewhat overlooked aspect of the characterization of technological superconductors in sole terms of their I_c is that this is just one of the parameters derived from the full *IV* curve measurement that provides the true characterization. As revealed by Eq. (4), the second parameter of relevance is the *n* value, or the exponent of the *IV* curve. Comparison of results obtained solely for I_c presupposes, strictly, that the *n* value of all the measurements is the same. This is of particular importance given that an entirely arbitrary voltage criterion is used to define I_c. In the case where the *n* value differs between measurements, there is the potential at least that the selection of different voltage criteria could lead to different behavior of the sample being presented. This is exemplified in the data set shown in Figure 15, where it can be seen that the *n* value

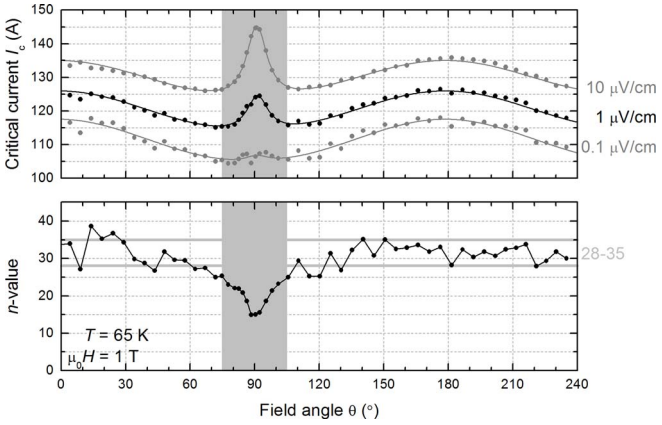

FIG. 15. Effect of varying *n* value on perceived I_c variation under the selection of different voltage criteria. Example data shown for a 65 K, 1 T angular I_c dependence of a HTS coated conductor wire.

diverges sharply from its usual value of ∼30 in precisely the vicinity of the 90° peak in I_c, reaching a value at the peak less than half its usual value elsewhere. The consequence of this in terms of the *IV* curves is clear: by selecting a lower voltage criterion, commonly thought to more properly represent the true behavior, the I_c peak can be made to vanish almost completely. Conversely, selection of a higher voltage criterion, for example the 10 μV/cm that is also often used, serves to strongly emphasize the peak. This is not an uncommon occurrence in coated conductor samples, and deserves greater investigation, particularly in view of the increasing relevance of the *n*-value itself as a characterization parameter in emerging applications such as nuclear magnetic resonance magnets.

We predict that a more in-depth study of *n* values will arise as a result of the greater measurement efficiency of a characterization system such as this one; as more complete data sets are made available; and as researchers strive to understand the I_c variations that they observe in different samples across the full breadth of the parameter space.[23–25]

VII. FUTURE DEVELOPMENT

As mentioned in Sec. II, a planned future development of the system is the substitution of a more powerful sample cryocooler to enable sample temperatures of 10 K or lower to be attained, increasing the attractiveness of the system for application to a wider range of superconducting materials of technological relevance, in particular MgB_2, and/or the combination of the two compressors presently required to separately power the two cold heads into a single unit. The operation of the sample cold head motor at 60 Hz (in a 50 Hz mains frequency country) has been trialed and demonstrated to offer a marginal improvement in the achievable base temperature at a minimal additional cost.

A further planned extension of the system is an increase in the sample rod length to accommodate samples up to 12 cm in length. As previously noted, the size of sample able to be accommodated by the system is not presently a limiting size, and extension to longer samples will be beneficial to achieving good current transfer into the measurement region of the superconductor in the case where the wire is laminated with a poorly conducting strengthening material such as stainless steel.

Adaptations of the sample rod to specific functions (for example, in-plane field measurements, low current measurements, thermopower measurements) are eminently feasible, and a range of different sample rods optimized for different purposes may be appropriate. Finally, additional electrical measurement types such as $R(T)$, $R(H)$ (magnetoresistivity) and Hall effect should be possible using the existing hardware with the development of appropriate software to run the measurement, and will provide easy access to further superconducting material parameters such as the transition temperature T_c and the irreversibility field B_{irr}. While these additions will increase the versatility and general usefulness of the system, they are unlikely to encourage additional target applications beyond superconductor characterization since the primary design feature of the system is the high current capability, which is of limited relevance to these additional measurement types.

VIII. SUMMARY

A turn-key system for the routine characterization of second generation high temperature superconducting coated conductor tapes under the operating conditions of particular relevance to application has been designed and constructed. The system is also well suited to other types of superconducting wires such as first generation HTS[26] and to a more limited extent MgB_2. Results obtained using the system[27–29] have provided the most detailed characterization of presently-available wires reported to date in a measurement that requires no user intervention from start to finish. It is intended that the system will be commercially constructed and marketed by HTS-110 Ltd. for use by wire manufacturers and superconductor researchers. Individual components of the system such as the HTS magnet and the efficient liquid-cryogen-free low-temperature cooling system will also be able to be adapted for other purposes.

ACKNOWLEDGMENTS

This work has been supported by the New Zealand Ministry of Business, Innovation, and Employment. The authors are grateful to Donald Pooke of HTS-110 for his ongoing interest in and support of this development and to Shaun Bredenkamp and Marc Mulholland of the Callaghan Innovation mechanical workshop for their patient assistance in working through multiple iterations of the various mechanical parts required to successfully construct this instrument. We are also grateful to our many commercial wire manufacturer partners for providing us with diverse superconducting wire architectures upon which to test the system.

[1]M. W. Rupich, X. Li, C. Thieme, S. Sathyamurthy, S. Fleshler, D. Tucker, E. Thompson, J. Schreiber, J. Lynch, D. Buczek, K. Demoranville, J. Inch, P. Cedrone, and J. Slack, Supercond. Sci. Technol. **23**, 014015 (2010).
[2]V. Selvamanickam, Y. Chen, X. Xiong, Y. Y. Xie, M. Martchevski, A. Rar, Y. Qiao, R. M. Schmidt, A. Knoll, K. P. Lenseth, and C. S. Weber, IEEE Trans. Appl. Supercond. **19**, 3225 (2009).
[3]H. Kutami, T. Hayashida, S. Hanyu, C. Tashita, M. Igarashi, H. Fuji, Y. Hanada, K. Kakimoto, Y. Iijima, and T. Saitoh, Physica C **469**, 1290 (2009).
[4]V. Matias, E. J. Rowley, Y. Coulter, B. Maiorov, T. Holesinger, C. Yung, V. Glyantsev, and B. Moeckly, Supercond. Sci. Technol. **23**, 014018 (2010).
[5]A. Usoskin, L. Kirchhoff, K. Knoke, B. Prause, A. Rutt, V. Selskij, and D. E. Farrell, IEEE Trans. Appl. Supercond. **17**, 3235 (2007).
[6]S. Nishijima, S. Eckroad, A. Marian, K. Choi, W. S. Kim, M. Terai, Z. Deng, J. Zheng, J. Wang, K. Umemoto, J. Du, P. Febvre, S. Keenan, O. Mukhanov, L. D. Cooley, C. P. Foley, W. V. Hassenzahl, and M. Izumi, Supercond. Sci. Technol. **26**, 113001 (2013).
[7]P. Tixador, Physica C **470**, 971 (2010).
[8]Y. Iwasa, J. Bascuñán, S. Hahn, M. Tomita, and W. Yao, IEEE Trans. Appl. Supercond. **20**, 718 (2010).
[9]R. Fuger, M. Eisterer, and H. W. Weber, IEEE Trans. Appl. Supercond. **19**, 1532 (2009).
[10]U. P. Trociewitz, M. Dalban-Canassy, M. Hannion, D. K. Hilton, J. Jaroszynski, P. Noyes, Y. Viouchkov, H. W. Weijers, and D. C. Larbalestier, Appl. Phys. Lett. **99**, 202506 (2011).
[11]V. Selvamanickam, Y. Yao, Y. Chen, T. Shi, Y. Liu, N. D. Khatri, J. Liu, C. Lei, E. Galstyan, and G. Majkic, Supercond. Sci. Technol. **25**, 125013 (2012).
[12]Q. Wang, Y. Dai, B. Zhao, S. Song, Z. Cao, S. Chen, Q. Zhang, H. Wang, J. Cheng, Y. Lei, B. Ye, X. Li, J. Liu, S. Zhao, H. Zhang, X. Hu, C. Wang, L. Yan, and K. Kim, IEEE Trans. Appl. Supercond. **19**, 2325 (2009).
[13]M. H. Sohn, S. Kim, K. D. Sim, H. M. Kim, J. H. Bae, D. W. Ha, H. Y. Park, B. Y. Eom, and S. Choi, Physica C **471**, 1449 (2011); M.-H. Sohn, K. Sim, H.-J. Kim, B.-Y. Eom, Y.-W. Jeong, S.-K. Baik, and K.-C. Seong, "Design and manufacturing of a conduction-cooled sample holder for a superconducting property measurement system," in *Proceedings of the Applied Superconductivity Conference*, 10–15 August 2014 (IEEE Trans. Appl. Supercond, 2014).
[14]See http://www.hts-110.com for product information and specification.
[15]S. C. Wimbush and N. M. Strickland, "Cryogenic fluid circuit design for effective cooling," U.S. provisional patent 61/980,896 (17 April 2014).
[16]For example, the CryoFan range from CryoZone BV, see http://www.cryozone.nl.
[17]N. M. Strickland and S. C. Wimbush, "Cryogenic gas circulation and heat exchanger," U.S. provisional patent 61/980,337 (16 April 2014).
[18]C. Hoffmann, N. Strickland, D. Pooke, J. Gannon, B. Carter, and A. Otto, J. Phys.: Conf. Ser. **234**, 022015 (2010).
[19]SHI Cryogenics, CH-204 cold head capacity map, see http://www.shicryogenics.com//wp-content/uploads/2012/11/CH-204_Capacity_Map.pdf.
[20]S. C. Wimbush and N. M. Strickland, figshare, 2014, see http://dx.doi.org/10.6084/m9.figshare.1165595.
[21]N. M. Strickland, N. J. Long, E. F. Talantsev, J. A. Xia, J. Kennedy, A. Markwitz, A. Zondervan, M. W. Rupich, W. Zhang, X. Li, and S. Sathyamurthy, AIP Conf. Proc. **1151**, 82 (2009).
[22]S. C. Wimbush and N. J. Long, New J. Phys. **14**, 083017 (2012).
[23]L. Civale, B. Maiorov, J. L. MacManus-Driscoll, H. Wang, T. G. Holesinger, S. R. Foltyn, A. Serquis, and P. N. Arendt, IEEE Trans. Appl. Supercond. **15**, 2808 (2005).
[24]S. Oh, H. Choi, C. Lee, S. Lee, J. Yoo, D. Youm, H. Yamada, and H. Yamasaki, J. Appl. Phys. **102**, 043904 (2007).
[25]J. R. Thompson, Ö. Polat, D. K. Christen, D. Kumar, P. M. Martin, and J. W. Sinclair, Appl. Phys. Lett. **93**, 042506 (2008).
[26]S. C. Wimbush, N. M. Strickland, and N. J. Long, "Low-temperature scaling of the critical current in 1G HTS wires," IEEE Trans. Appl. Supercond. (published online).
[27]N. M. Strickland, S. C. Wimbush, J. V. Kennedy, M. C. Ridgway, E. F. Talantsev, and N. J. Long, "Effective low-temperature flux pinning by Au ion irradiation in HTS coated conductors," IEEE Trans. Appl. Supercond. (published online).
[28]N. M. Strickland, C. Hoffmann, S. C. Wimbush, D. M. Pooke, T. Huang, Z. Lazic, V. Chamritski, E. F. Talantsev, N. J. Long, and J. L. Tallon, J. Phys.: Conf. Ser. **507**, 022037 (2014).
[29]E. F. Talantsev, N. M. Strickland, S. C. Wimbush, J. G. Storey, J. L. Tallon, and N. J. Long, Appl. Phys. Lett. **104**, 242601 (2014).